Studies of Beam Intensity Effects in Fermilab Booster Synchrotron

Part I: Introduction; Tune and Chromaticity Scans of Beam Losses.

Vladimir Shiltsev, Jeff Eldred, Valery Lebedev, Kiyomi Seiya

Fermi National Accelerator Laboratory, PO Box 500, Batavia, IL 60510, USA

Abstract

Detrimental beam dynamics effects limit performance of high intensity rapid cycling synchrotrons (RCS) such as the 8 GeV Fermilab Booster. Here we report the results of comprehensive studies of various beam intensity dependent effects in the Booster. Part I covers the dependencies of the Booster beam intensity losses on the total number of protons per pulse and on key operational parameters such as the machine tunes and chromaticities. In Part II we cross-check two methods of the beam emittance measurements (the multi-wires proportional chambers and the ionization profile monitors), analyze the intensity dependent emittance growth effects and discuss the ultimate performance of the machine now and after foreseen and proposed upgrades.

PACS numbers: 29.20.D-, 29.20.Lq, 29.27.Bd, 29.27.Fh

1. BOOSTER SYNCHROTRON OPERATIONS AND MOTIVATION FOR STUDIES

The complex of Fermilab proton accelerators includes a 750 keV H- RFQ, 400 MeV *H-* pulsed normal-conducting RF linac, 8 GeV proton Booster synchrotron , 8 GeV Recycler storage ring that shares tunnel with 120 GeV proton Main Injector synchrotron, and a 3.1 GeV muon Delivery Ring [1, 2]. Some 16 km of beamlines connect the accelerators, bring the beams to fixed targets and to experiments for high energy particle physics research at the Intensity Frontier with a world-record 750 kW of average 120 GeV beam power on the neutrino target achieved in 2019. There are plans to further increase the power to over 1.2 MW beam power on target at the start of the LBNF/DUNE experiment [3] in the middle of the 2020's via replacement of the existing 40 years old 400 MeV normal-conducting Linac with a modern CW-capable 800 MeV superconducting RF linear accelerator (PIP-II, see [4]) located inside the now defunct Tevatron ring [5] and corresponding beamline for injection into the Booster. There are also several concepts to further double the beam power to >2.4 MW after replacement of the existing 8 GeV Booster synchrotron [6-7].

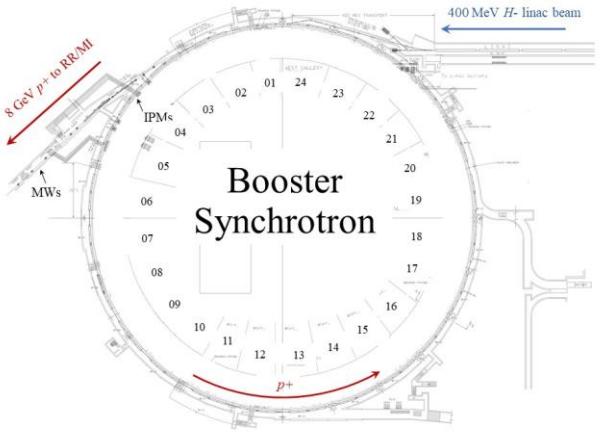

Figure 1: Fermilab Booster synchrotron. Sectors, each cosnisting of four magnets, are numerated 1 to 24. Indicated are locations of the Ionization Profile Monitors (IPMs), Multi-Wire (MW) beam profile monitors in the 8 GeV proton transport line to the Recycler/Main Injector and the 400 MeV H^- beam injection line.

The Fermilab Booster [8] is a 474.2 m circumference, alternating-gradient, rapid-cycling synchrotron (RCS) containing 96 combined-function magnets – see Fig.1. Together with capacitor banks, these magnets form a resonant network and get excited with a 15-Hz biased sine wave. Beam acceleration ramp from 0.4 GeV at injection to 8.0 GeV at extraction is 33.3 ms long - half of the magnet cycle period – and contains about 20 000 turns. Correspondingly, all the parameters of the machine and beam significantly vary in the cycle – from the currents in all correctors (trim dipoles, trim quads and skew quads, sextupoles and octupoles) to RF frequency, voltage and phase (see Fig.2), from the betatron and synchrotron tunes and chromaticities to proton beam intensity, positions, sizes, emittances, bunch length and energy spread, etc. Main parameters of the Booster are given in Table 1. Without going into details of the Booster high intensity operation and interface with other machines in the complex which can be found in Refs. [9 - 11], here we only briefly outline main processes which occur at injection, transition crossing and extraction.

Table 1: Main parameters of the Fermilab Booster rapid cycling proton synchrotron.

Parameter				Comments
Circumference	C	474.20	m	
Injection energy (kinetic)	E_i	400	MeV	$\beta_i=0.701$, $\gamma_i=1.426$
Extraction energy (kinetic)	E_f	8	GeV	$\beta_f=0.994$, $\gamma_f=9.526$
Cycle time	$T_0=1/f_0$	1/15	s	beam cycle 20,000 turns
Harmonic number	h	84		
RF frequency at inj. – extr.	f_{RF}	37.77-52.81	MHz	
RF voltage (max.)	V_{RF}	1.1	MV	
Transition energy (kinetic)	E_{tr}	4.2	GeV	$\gamma_{tr}=5.478$, at t=17ms
No. of cells, bend magnets	P	24, 96		*FOFDOOD, 96º/cell*
Typical total intensity	N_p	4.5	10^{12}	in N_b=81 bunches
Typical rms norm. emittance	$\varepsilon_{x,y}$	2.0π	μm	12π μm for 95%
Optics functions (max.)	$\beta_{x,y}$, D_x	33.7/20.5/3.2	m	design values

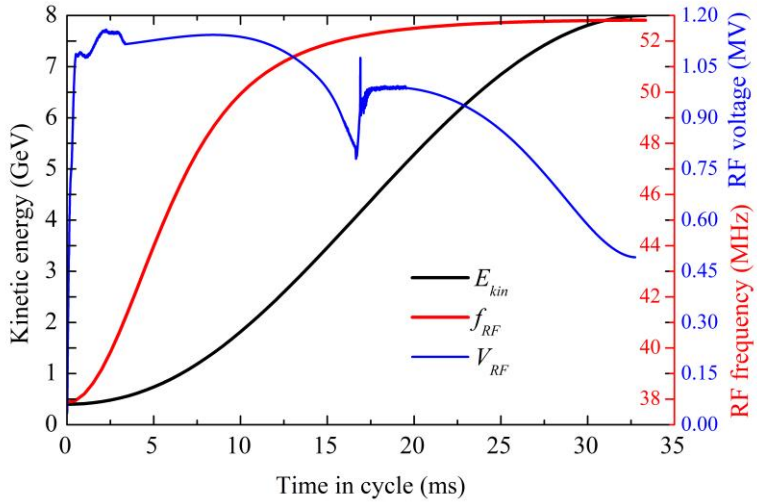

Figure 2: Booster ramp: kinetic energy (black), RF voltage(blue) and frequency (red).

The Booster receives 400 MeV H^- beam of 201 MHz bunches from the Linac while it is close to minimum of the magnetic field ramp. H^- particles are stripped of two electrons when pass through a thin foil and resulting protons are accumulated over many turns in the ring (the scheme known as charge exchange injection). Correspondingly, the total injected and accelerated beam intensity N_p scales with the Linac current, which is typically ~25 mA, and the total number of injection turns N_{turns}, approximately as $N_p=0.35\cdot10^{12}\cdot N_{turns}$, e.g., about $4.9\cdot10^{12}$ for a typical 14-turn injection. The duration of the beam injection also scales with the number of turns s $2.2\cdot N_{turns}$ [μsec]. The beam is injected with RF voltage close to zero and then adiabatically captured over about 300 μsec by the RF system [12]. Right after injection and in the following several milliseconds, the high intensity protons beam is subject of the strongest space-charge forces, characterized by the space-charge parameter ΔQ_{SC}~0.4. Transverse and longitudinal ring impedances are large [13-15] and the Booster operation requires simultaneous, fast and idiosyncratic adjustment of orbits, optical

functions [16], tunes, chromaticities and many other machine parameters on top of changing energy, RF voltage and frequency (see Fig.3).

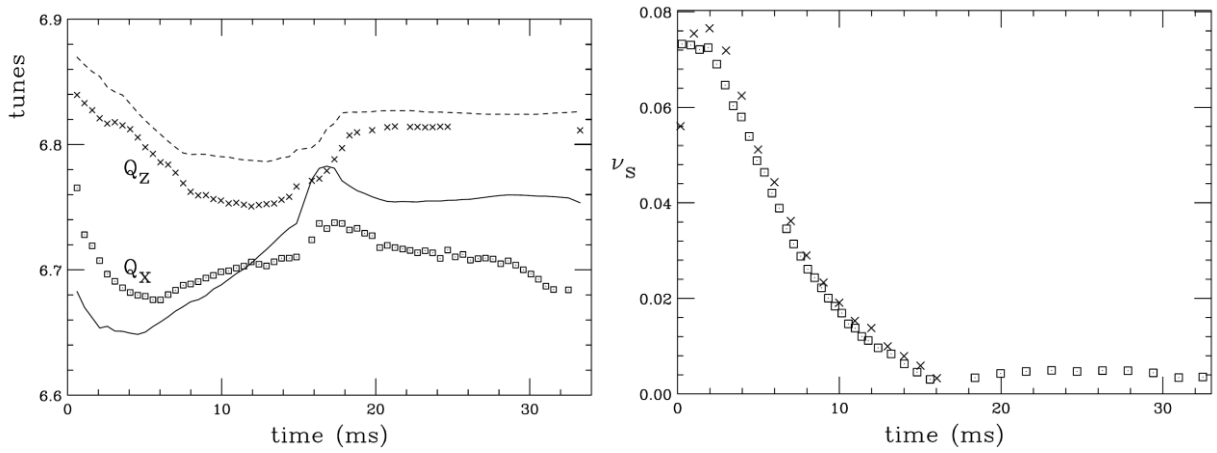

Figure 3: Booster tunes: a) left - The horizontal (square) and vertical (cross) betatron tunes in a booster cycle. Tunes calculated by MAD model are compared to measurements (solid and dashed lines); b) right - The synchrotron tune in the Booster cycle. The squares are measured from turn-by-turn data with ICA method (from [17]).

In the Booster, transition occurs at an energy of ~4.2 GeV and occurs at about 17 msec in the Booster cycle. The Booster is currently operated without a dedicated γ_t jump system, though the current of trim quadrupoles varies at maximum rate at the transition to get through it as fast as possible and the RF system voltage and frequency follow complicated curves in order to minimize the losses and control the longitudinal emittance, which somewhat grows from its initial 95% value of about 0.08 eVs [18-20].

The rapid acceleration of the Booster requires large accelerating voltage which results in a large momentum spread relative to its temporal spread. To inject the Booster beam efficiently into the Recycler for slip-stacking, it is desirable to rotate the beam in longitudinal phase-space so that it has a smaller momentum spread [21]. The Booster bunch rotation is performed via quadrupole excitation of the synchrotron oscillation as the RF voltage is modulated at twice the synchrotron

frequency and this drives a longitudinal quadrupole resonance. Once the beam energy is close to the extraction energy we perform snap bunch rotation, i.e., at about 2 msec before the end of the cycle, the RF voltage is increased slowly to ≈650 kV to increase the energy spread of the bunches and dropped down rapidly to ≈ 130 kV. This gives minimum energy spread for the beam for slip stacking in the downstream accelerators.

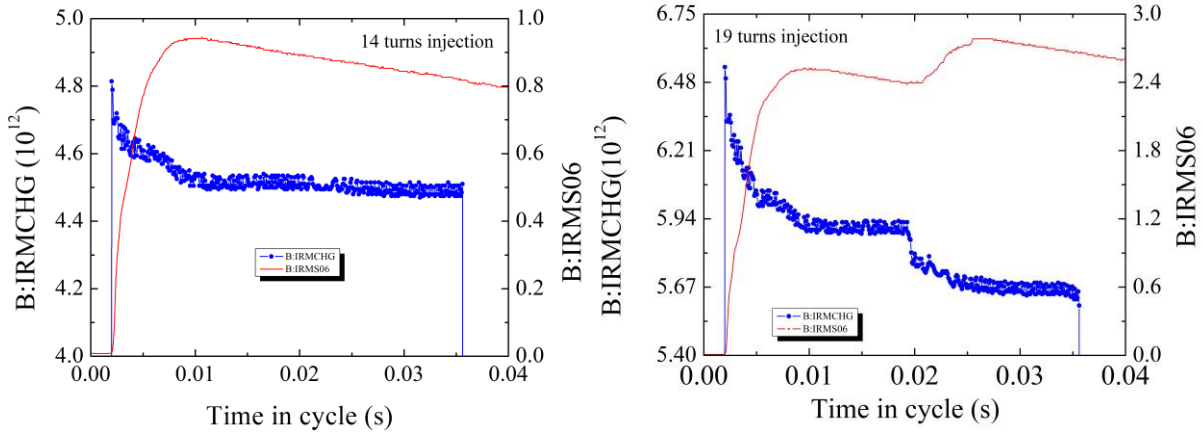

Figure 4: Booster beam losses: a) left – the intensity monitior BCHG0 signal (blue, left axis) and the S06 BLM readings (red, right axis) over the cycle with usual 14 turns injection intensity; b) right – the same for higher intensity 19 turns injection.

The overall average Booster beam loss limit has been administratively set to W =525W, i.e., 35J per cycle with 15 Hz beam cycles. Such level allows us to maintain all elements in the Booster tunnel without excessive radiation exposure and corresponds to either 13% beam loss at injection energy or 1.2% at the transition, or 0.6% at extraction for nominal intensity of about $4.5 \cdot 10^{12}$ protons per pulse. As illustrated in Fig.4, at nominal intensity, with 14 turns injection, the losses mostly occur at injection, but the loss at transition becomes dominant at higher intensities. In general, the beam loss induced radiation is the most important and most challenging factor limiting the performance of high intensity RCSs [22]. Indeed, if the tolerable uncontrolled radiation level in

accelerator enclosures is set at $W=f_0\int E_k\, dN_p$ (typically about 1 W per a meter of machine circumference), then the fractional beam loss must be kept under

$$\frac{\Delta N_p}{N_p} \leq \frac{W}{(1-\eta)N_p E_k f_0}\ , \qquad (1)$$

where η is the efficiency of the collimation system that directs the losses into dedicated beam absorbers or dumps [23, 24]. Obviously, the loss tolerances get tighter with the increase of beam intensity, energy and power. However, many beam physics phenomena, such as, e.g., repelling forces of the proton beam's own space-charge (SC) lead to increase of beam sizes and particle losses at higher beam intensities. In circular rapid cycling accelerators, an empirical *space-charge parameter* (the core particle tune shift):

$$\Delta Q_{SC} = \frac{N_p r_p B_f}{4\pi\varepsilon\beta\gamma^2}\ , \qquad (2)$$

is observed to be limited at 0.3-0.4. Here N_p is the total intensity assuming that the bunches fill all h RF buckets, r_p is the classical proton radius, B_f is the bunching factor – the ratio of the peak to average bunch current, approximately equal to $(2\pi)^{1/2}/\varphi_{rms}$, for the rms bunch φ_{rms} duration in the units of radians of the RF phase - ε is the normalized beam emittance, β,γ are relativistic Lorentz factors. Beyond the limit, the losses grow unacceptably with increase of the beam intensity beyond that set by Eq.(2). Of course, the scaling of Eqs.(1) and (2) are absolutely opposite – the first one calls for smaller losses at high intensity while the second one assumes the losses growing with the

intensity. To illustrate that, one can assume the space-charge induced losses grow with the space-charge tuneshift, for example, as:

$$\frac{\Delta N_p}{N_p} \sim \alpha \Delta Q_{SC}{}^{\kappa} \quad , \quad (3)$$

then, following [25] one gets from Eqs.(1) and (2) for the maximum intensity within the loss power limit W:

$$N_p^{max} \sim \left(\frac{W}{1-\eta}\right)^{\frac{1}{\kappa+1}} \cdot \left(\frac{\varepsilon}{B_f}\right)^{\frac{\kappa}{\kappa+1}} \cdot \gamma^{\frac{3\kappa}{\kappa+1}} \cdot (\alpha f_0)^{-\frac{1}{\kappa+1}} \quad . \quad (4)$$

Correspondingly, as summarized in Ref.[26], the paths to increase the maximum intensity usually include: a) better collimation systems to increase η; b) larger emittance within the available machine aperture; c) flatten the bunches longitudinally to reduce B_f, for example, by using the 2nd or 3rd harmonics RF ; d) increase the injection energy; e) reducing the losses via beneficial beam dynamics improvements that would make α and κ smaller, e.g., by the injection "painting" to make the SC force more uniform, or via the SC compensation using electron lenses, or by implementation of the non-linear integrable optics, etc.

Naturally, a better understanding of the particle loss observables and mechanisms is of great importance and was always in the focus of the Booster operation experts [27]. Here we report the results of the beam loss and beam emittance studies carried out as part of the Summer 2019 "Booster Beam Physics Studies Program" [28]. The first part of the report deals with the intensity diagnostics and loss measurements. Part II is to follow and to address the intensity dependent emittance growth in the Booster beams.

2. BOOSTER INTENSITY AND LOSS MONITORS

The main diagnostics of the total circulating Booster beam intensity is the ACNET channel B:CHG0, that uses the signal from the beam current toroid properly mixed and averaged with the RF waveform signal. Frequency of the latter is quickly changing in time - see Fig.2. The results of the fractional loss vs injected beam intensity scans, under typical operational conditions (i.e. by changing only the number of turns at injection) are shown in black dots in Fig. 5. The data represented the fractional changes after 8 ms of the Booster cycle and at the extraction (at 33 ms). One can see that over wide range of initial intensities these data are about the same, indicating that the losses occur mostly at and right after the injection – as it is clearly seen in Fig.4 a). The difference reflects the additional intensity loss of about 0.5-1% that takes place at the transition. Those losses become significant at $N_p > 6 \cdot 10^{12}$ ppp (particle per pulse).

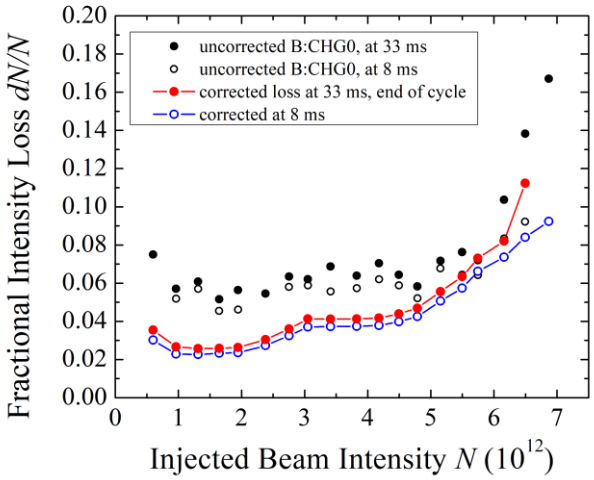

Figure 5: Fractional Booster beam intensity losses vs total injected number of protons: black circles and dots – for raw B:CHG0 intensity data taken at 8 ms in the cycle and at extraction, respectively; blue circles and red dots – for the data corrected for the toroid systematic error (see text).

The raw B:CHG0 toroid intensity data need to be corrected, though. There are subtle features of the signal indicating several % systematic variations early in the cycle, as shown in Fig.4 a) where high resolution toroid signal shows not only general trend but also unphysical signal increases. The working hypothesis is that the effect is due to the processing of quickly changing signals early in the cycle and the toroid frequency response causing unexpected variation on the signal after the notch is created in the beam pulse. There several possible ways to recalibrate or fix the problem. We have carried out a cross calibration of the intensity loss ΔN_p reported by B:CHG0 and the power loss signal measured by one of the most appropriate beam loss monitors BLMS06 – see Fig.6 b) [29].

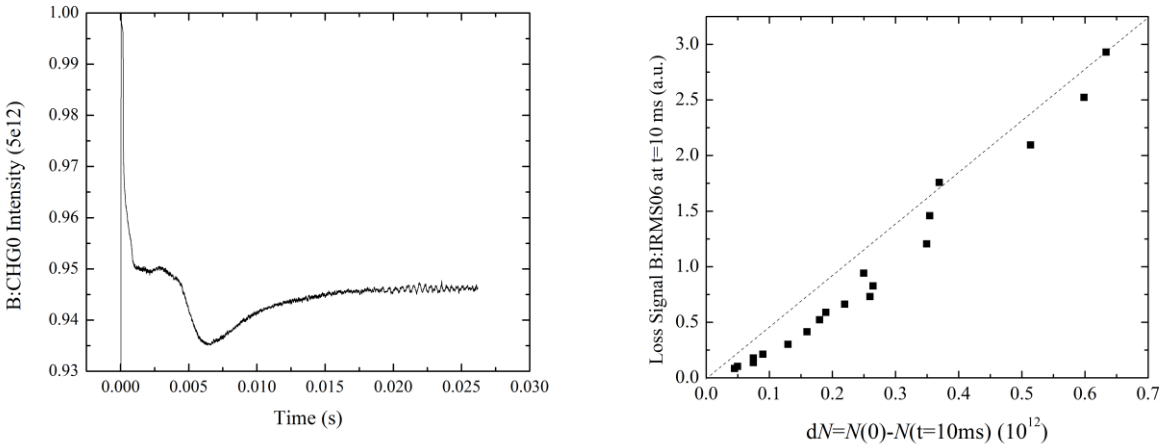

Figure 6: a) left – reported B:CHG0 intensity, normalized to $5 \cdot 10^{12}$, in the Booster cycle; b) the BLMS06 signal as measured at 10 ms into the Booster cycle vs the beam intensity change in the same 10 ms as measured by the B:CHG0 intensity monitor. The dashed line indicates the linear dependence anticipated from high beam intensity loss measurements.

As shown in Fig.4, the BLMS06 signal has much more narrow bandwidth and reaches its peak at 10 ms into the cycle with the amplitude proportional to the power loss integrated well over the initial lossy period of the Booster cycle. The loss monitor signals at 10 ms are compared to the reported changes in the toroid signal B:CHG0 – see Fig. 6 b) - and one finds that the latter

significantly overestimates the losses at small intensities but that difference disappears (mutual linearity gets restored) at high losses. Application of such systematic correction to the B:CHG0 data (some 60% reduction at lower intensities) results in solid lines in Fig. 5. The total losses at small intensities are now at the range of 2-3% instead of 5-6% without the correction; the fractional losses at the operational intensities ~$4.4 \cdot 10^{12}$ are only 4-4.5% (vs 6-7%) and the losses at higher total intensities are mostly unchanged.

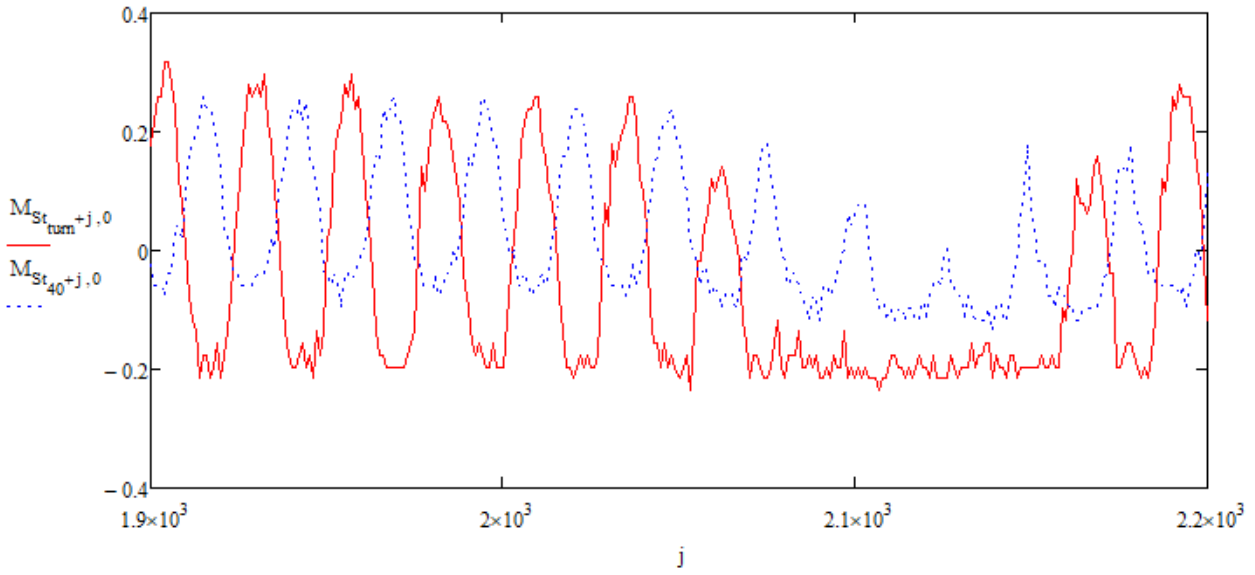

Figure 7: Booster RW monitor traces for the bunch beam current profiles right before (dashed blue) and 40 turns after (solid red) the extraction gap clearing.

As we are interested in the intensity dependent beam loss, one more correction to the data shown in Fig.5 is needed to account for the notch clearing. The Booster extraction kicker rise time is about 70 ns long and to reduce the losses at extraction one needs to avoid any beam in that interval, i.e., a beam gap is required. Out of the total loss budget *W* consideration, such a gap, equivalent to removing 3 out 84 possible Booster bunches, is created at low beam energies. First, a laser system [30] is being built to create the notch within a Linac beam pulse, immediately after the RFQ at 750 keV, where activation issues are absent. The beam with such a gap is injected into the

Booster. Unfortunately, the laser notch system is not 100% efficient and, in addition, some particles slip into the gap before the injection RF capture and as the result there is some 400 MeV beam in the gap – as illustrated by Fig. 7. These particles are cleared out at approximately 150 turns after the injection by a kicker pulse that removes some 1-2% of the total beam intensity. In the future, it is expected that the laser notcher power increase will greatly reduce the number of unwanted particles in the gap.

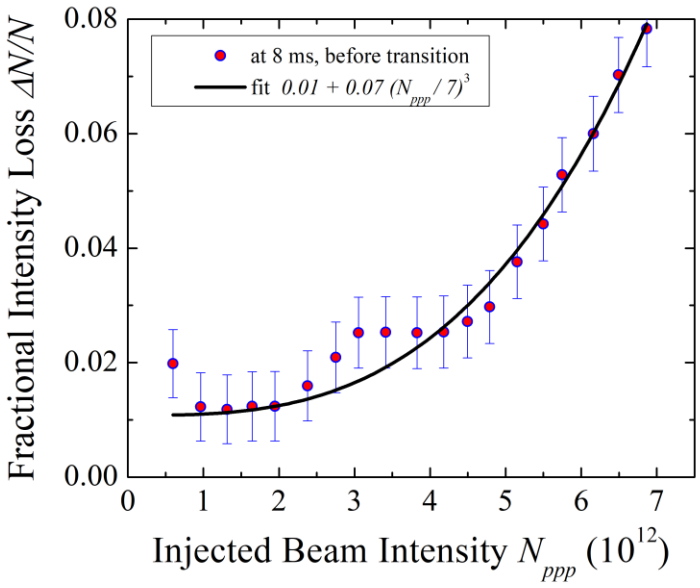

Figure 8: Intensity-dependent fractional Booster beam intensity loss at injection vs total number of protons.

In any case, the loss of 1.4±0.4% of the total intensity out of the extraction gap is not related to intensity dependent effects we are after, and it should be taken out of the Fig.5 data. The resulting fractional intensity-dependent Booster beam loss is presented in Fig.8. As one can see, the losses quickly grow with N_p – solid line in Fig.8 is for fit

$$\frac{\Delta N_p}{N_p} = 0.01 + 0.07\,(\frac{N_p}{7\times10^{12}})^3 \quad , \qquad (5)$$

While the chosen functional dependence is similar to Eq.(3), it is not substantiated by theory or modeling, and could be improved (for example, to a threshold-like one), the non-zero intercept at small N_p might be either be indicator of a different mechanism of constant losses at low intensity or just due to limited measurement accuracy.

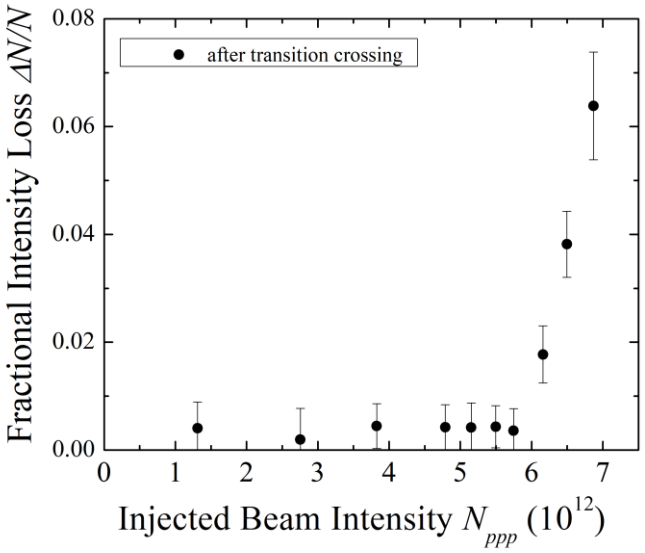

Figure 9: Intensity-dependent fractional beam intensity loss at transition vs total number of protons.

The beam intensity losses at the transition crossing have a threshold at about $6 \cdot 10^{12}$ ppp as shown in Fig. 9. The characteristic dependence is quite different from what is observed at the injection and clearly points to different beam physics mechanisms underlying these phenomena. We also have to note that there is no automatic phase or frequency adjustment for transition. If there are beam loading effects at transition, the transition crossing has to be retuned, while during our studies we did not retune the transition. All in all, the beam losses in the Booster at the record high injected intensity of $7 \cdot 10^{12}$ ppp are about $1 \cdot 10^{12}$, that is about 15% of the total - see Fig.10. Obviously, such losses are not acceptable for routine operation within the administrative beam power loss limit.

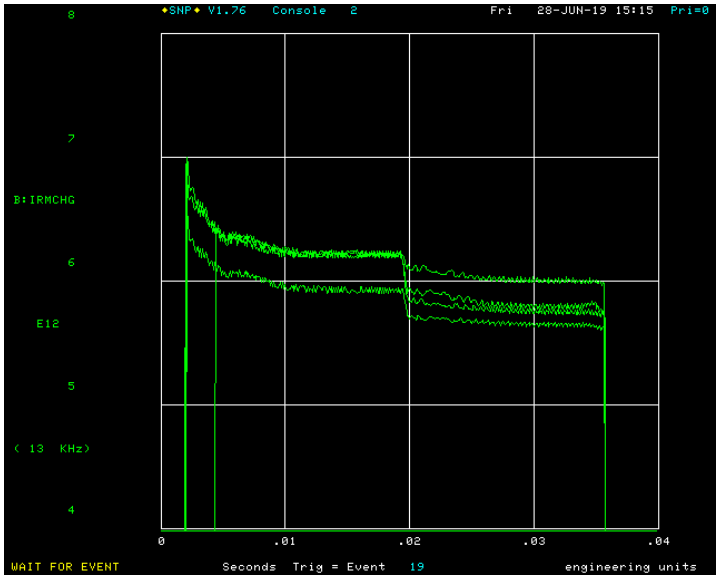

Figure 10: The record Booster beam intensity plot, indicating the transmission improvements after the tuneup at the transition energy crossing (see text).

3. TUNE AND CHROMATICITY SCANS

To better understand the nature of the intensity loss phenomena we have studied the Booster transmission efficiency dependence on the chromaticities and tunes - the $Q_{x,y}'$ and $Q_{x,y}$ scans. Fig. 11 shows the dependence of the losses over the first 1 ms of the Booster cycle (~450 turns) at the nominal operational tunes $Q_{x,y}$= 6.78/6.88 but at three different chromaticity settings – the nominal one $Q'_{x,y}$=-4/-16, and then at $Q'_{x,y}$=-12/-12, and at $Q'_{x,y}$=-20/-20. The fractional losses were calculated out of the B:CHG0 signal, corrected for the systematic error at lower intensities and with the extraction gap clearing loss subtracted, following the method presented in the preceding section.

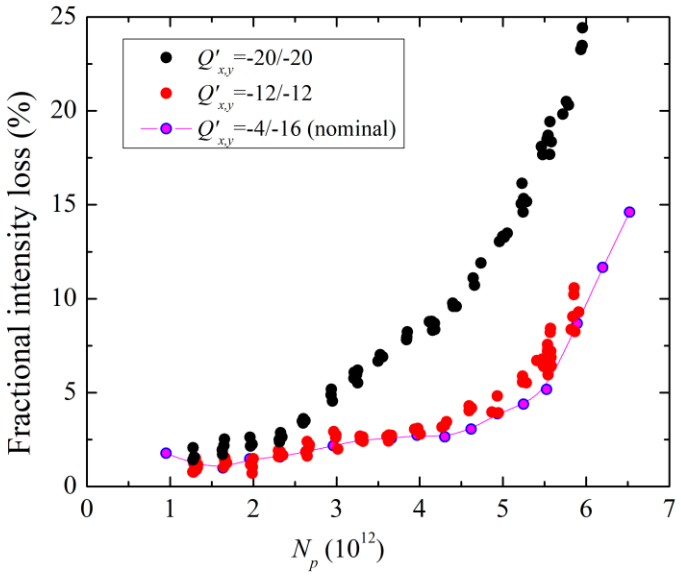

Figure 11: Trasmission effieciency 1 ms after injction for different chromaticities $Q_{x,y}'$ vs N_p.

The results are presented in Fig.11 and clearly show significant increase of the losses with the chromaticity. Taking for simplicity the same functional dependence on intensity as in Eq.(5), the data can be approximated as

$$\frac{\Delta N_p}{N_p} = (0.013 \pm 0.003) + (0.10 \pm 0.02)\left(\frac{N_p}{7\times10^{12}}\right)^3\left(\frac{<Q'>}{10}\right)^{1.9\pm0.2}, \qquad (6)$$

with $<Q'> = (|Q_y'| + |Q_y'|)/2$ denoting the average chromaticity. There is a lower limit on operational chromaticity that depends on the intensity and is usually asociated with the need to maintain the coherent beam stability. Correspondingly, the low chromaticity operation is possible only at low intensities. Notably, the strong dependence of the losses at injection, presumably due to the space-charge effcets, $\Delta N_p \sim Q'^2$ – see Eq.(6) - are similar to the incoherent beam losses due to parasitic beam-beam effects observed in the Tevatron collider [31].

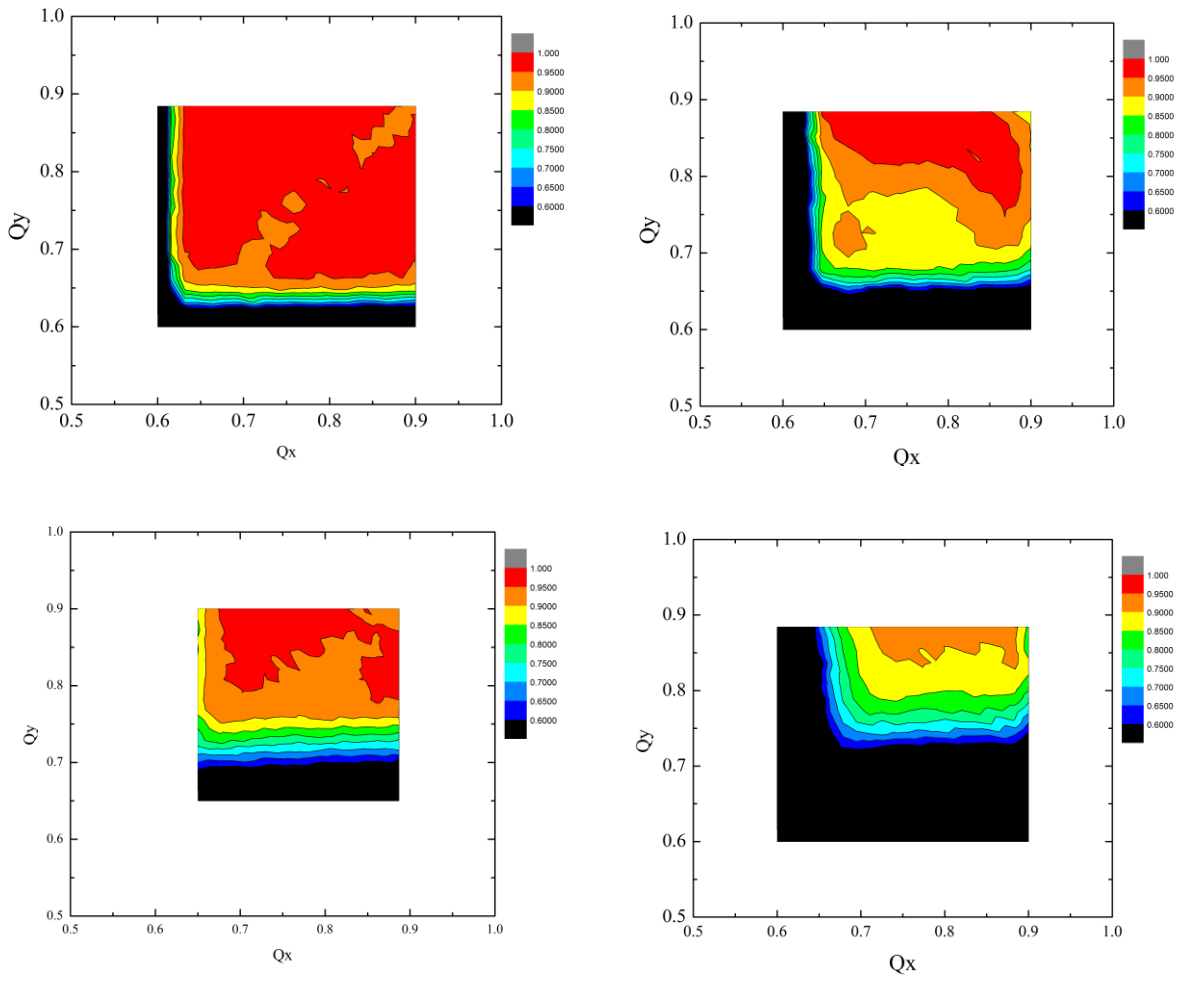

Figure 12: Tune scans of the trasmission efficiency over the first millisecond after injection: (top left) at the N_p=0.95·10^{12} and $Q_{x,y}$'=-6/-6; (top right) N_p=0.95·10^{12} and $Q_{x,y}$'=-20/-20; (bottom left) N_p=4.3·10^{12} and $Q_{x,y}$'=-4/-16; (bottom right) N_p=4.3·10^{12} and $Q_{x,y}$'=-20/-20.

The tune scans were carried out under six different conditions: i) low intensity and low chromaticity: N_p=0.95·10^{12}, $Q_{x,y}$'=-6/-6; ii) low intensity and high chromaticity: N_p=0.95·10^{12}, $Q_{x,y}$'=-20/-20 ; iii) high intensity and medium chromaticity: N_p=4.3·10^{12}, $Q_{x,y}$'=-12/-12; iv) high intensity and high chromaticity: N_p=4.3·10^{12}, $Q_{x,y}$'=-20/-20; v) medium intensity and medium chromaticity: N_p=2.6·10^{12}, $Q_{x,y}$'=-12/-12; vi) medium intensity and high chromaticity: N_p=2.6·10^{12}, $Q_{x,y}$'=-20/-20. Note, that vertical and horizontal tunes and chromaticities varied only

for the time period of 2 ms after the injection, and for the rest of the Booster cycle, they stayed as for the routine operational cycles.

The results of the first four are presented in Fig. 12. One can see that, in general, an increase of either the chromaticity or intensity or both leads to reduction of the available tune space for low loss operation and generally lower optimal transmission efficiencies. Table I summarizes the findings.

Table I: Optimal working points for various injected intensities and injection chromaticities: first line in each box – the minimal intesity loss 1 ms after injection (raw B:CHG0 data, uncorrected for the B:CHG0 systematics and the notcher gap cleaning) and the optimal horizontal and vertical tunes Q_x/Q_y; the second line – same for the entire Booster cycle (at extraction).

	$Q_{x,y}$'=-6/-6	$Q_{x,y}$'=-12/-12	$Q_{x,y}$'=-20/-20
N_p=0.95·10^{12}	1.5%, 0.68/0.84 3.5 %, 0.82/0.81		1.2%, 0.69/0.88 2.6 %, 0.77/0.88
N_p=4.3·10^{12}		3.0%, 0.74/0.87 7.0 %, 0.80/0.90	7.0%, 0.77/0.88 (6 %, 0.77/0.88

The tune scan data reveal stronger sensitivity of the losses to the vertical tune than to the horizontal one. For example, 14-units increase of the chromaticity from -6 to -20 at N_p=0.95·10^{12} resulted in the reduction of the 90% transmission tune area by dQ_y=0.05 in vertical plane while dQ_x=0.02 – see – see Fig.12 a) and b). Similarly, the change of the chromaticity from -12 to -20 for N_p=4.3·10^{12} led to shrinkage of the 90% transmission tune area by dQ_y=0.1 and dQ_x=0.05, as depicted in Fig.12 c) and d). That indicates a strong vertical resonance limitation.

4. DISCUSSION, PROJECTIONS FOR BOOSTER IN PIP-II ERA

Our 2019 beam studies of the Booster beam losses expose three effects: 1) some minor intensity-independent loss at injection ~1%; 2) significant $O(5\%)$ loss shortly after the injection that is due to space-charge effects as it strongly depends on the intensity, approximately as N_p^3, on the working point tunes $Q_{x,y}$ and on the chromaticities $Q_{x,y}'$; and 3) threshold-like increase of the losses during and after the transition $O(5\%)$ above $N_p=6\cdot10^{12}$. The first effect could be, e.g., due to the Booster aperture restrictions but is not very prominent within the intensity measurement error of ~1%. The accurancy of the intensity monitors needs to be significantly improved, especially at lower intensities, before further studies of the dependence of that effect on the Booster beam positions and emittances can be performed. The losses at the transition are probably indicative of complicated 3D dynamics of some kind of coherent instability [32]. Future investigations of the dependence on the chromaticities, tunes and other machine parameters will help to better identify the transition loss origin.

The space-charge induced losses in the first few thousands turns after the injection are very prominent and supposedly should be dependent on the space-change tune shift Eq.(2). The latter scales with $1/\beta\gamma^2$ and the bunching factor B_f – both of which are very quickly changing in time after the injection. For example, the measured rms bunch length φ_{RF} (in the units of the RF phase) – see Fig.13 - shows quite complex dynamics, that consequently results in fast variations of $B_f=(2\pi)^{1/2}/\varphi_{\mathrm{RF}}$. Correspondingly, the caluculated space-charge tune shift parameter first grows due to bunching after the injection, then falls down due to acceleration and exhibits some temporal increase at the transition – see Fig.14. As for do not know the exact dynamics of the beam emittance (subject of the following Part II of our report), the shadowed area in Fig.14 presents a range of the tuneshift parameters ΔQ_{SC} corresponding to the range of the transverse rms normalized

beam emittance of ε=2π mm mrad to 3π mm mrad. Assuming the growth of the emittance from injection to extraction withing this range, the dashed lin ein Fig.14 represents schematically the Booster tuneshift paramter that can reach as high as 0.4 or more sometime early in the acceleration cycle. Naturally, the corresponding incoherent space-charge tune spread does no fit the available tune space and that results in strong resonant excitation of participle's dynamics and eventually losses at the machine aperture.

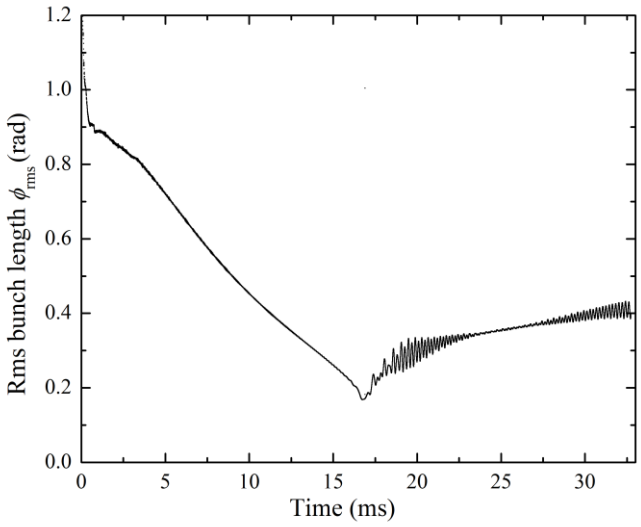

Figure 13: Booster rms proton bunch duration over the beam acceleration ramp.

Using the scaling law Eq.(4) with the exponent κ≈3 as in Eqs.(5) and (6), one can project torelable space-charge induced injection losses for the Booster operation in the PIP-II era with intensities up to N_p=4.3·10^{12} (γ_2/γ_1)$^{3\kappa/(\kappa+1)}$ ≈7.6·10^{12} , as the energy at injection will increase (so γ_2=1.8 instead of γ_1=1.4 now). The design intensity of N_p=6.5·10^{12} relatively safely fits this limit. Nevertheless, the actual Booster performance will also depend on the beam emittances with the new SRF injector linac. Also, the losses at the transition might pose very serious threat to safe operation as well.

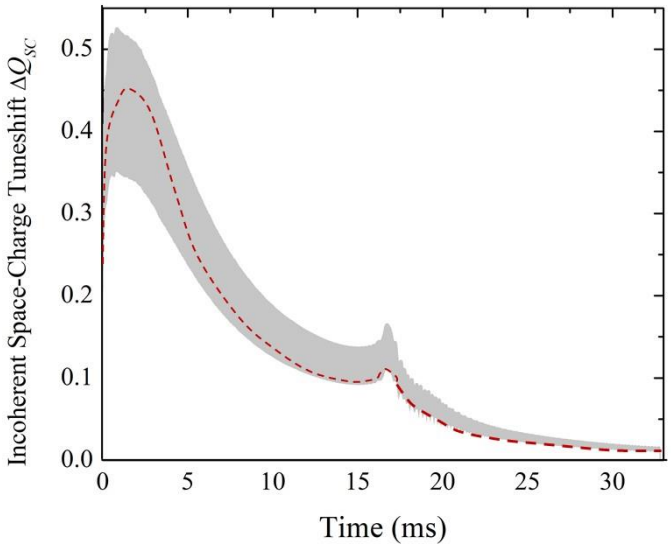

Figure 14: Range of the space-charge tuneshift parameters for a nominal intensity Booster beam cycle with N_p=4.3·10^{12}. The upper limit corresponds to the transverse rms normalized beam emittance of ε=2π mm mrad and the lower limit is for ε=3π mm mrad (see text).

ACKNOWLEDGEMENTS

We would like to thank C.Y. Tan, C. Bhat, Yu. Alexahin, A. Burov, W. Pellico and R. Thurman-Keup for numerous discussions on the topics of this study and S. Chaurize, V. Kapin and K. Triplett for their invaluable help with experimental Booster beam studies. In addition, the Summer 2019 Booster beam study campaign involved N. Eddy, C. Jensen, J. Larson, and H. Pfeffer of Fermilab, H. Bartosik, N. Biancacci, M. Carla, A. Saa Hernandez, A. Huschauer, F. Schmidt of CERN, D. Bruhwiler, J. Edelen of the Radiasoft SBIR company and V. Kornilov of GSI. We greatly appreciate their fruitful cooperation and the spirit of international beam physics collaboration.

Fermilab is supported by U.S. Department of Energy, Office of Science, Office of High Energy Physics, under Contract No. DE-AC02-07CH11359.

REFERENCES

[1] V.Shiltsev, Modern Physics Letters A, 32(16), 1730012 (2017)

[2] M. Convery, M.Lindgren, S.Nagaitsev, V.Shiltsev, Fermilab Accelerator Complex:

Status and Improvement Plans, Preprint FERMILAB-TM-2693 (2018).

[3] DUNE Collab., *Long-Baseline Neutrino Facility (LBNF) and Deep Underground Neutrino Experiment (DUNE) Conceptual Design Repor*t, arXiv:1601.05471

[4] V.Lebedev (ed.), The PIP-II Conceptual Design Report, Preprint FERMILAB-DESIGN-2017-01; FERMILAB-TM-2649-AD-APC (2017)

[5] V. Lebedev, V. Shiltsev, eds., *Accelerator Physics at the Tevatron Collider* (Springer, 2014)

[6] J. Eldred, et al., JINST, 14, P07021 (2019)

[7] J.Eldred, arXiv: 2001.05576

[8] E.L.Hubbard (ed.), "Booster Synchrotron", Preprint FERMILAB-TM-405 (1973);. The Booster injection energy was increased to 400 MeV in 1990, see ''Fermilab Linac Upgrade Conceptual Design,'' Fermilab Memo, Fermilab-LU-Conceptual Design (1989).

[9] *Booster Rookie Book*, https://operations.fnal.gov/rookie_books/Booster_V4.1.pdf

[10] J. Eldred, PhD Thesis, FERMILAB-THESIS-2015-31 (2015)

[11] C.Bhat, in *Proc. IPAC2015* (Richmond, VA, US), pp.3976-3978

[12] C.Bhat, in *Proc. HB2016* (Malmo, Sweden), pp.293-298

[13] K.Y.Ng, *Physics of intensity dependent beam instabilities* (World Scientific, 2016).

[14] A.Macridin, et.al., "Coupling impedance and wake functions for laminated structures with an application to the Fermilab Booster," Phys.Rev.ST Accel.Beams 14 (2011) 061003

[15] A.Macridin, J. Amundson, P. Spentzouris, V. Lebedev, T. Zolkin, (2013). *Transverse Impedance and Transverse Instabilities in Fermilab Booster*, Preprint FERMILAB-CONF-13-431 (2013)

[16] A.Valishev, Y. Alexahin, and V. Lebedev, Suppression of Half-Integer Resonance in FNAL Booster and Space Charge Losses at Injection, in Proc. HB2016, Malmö, Sweden (2016), pp.164-168

[17] X.Huang, S.Y. Lee, K.Y. Ng, Y. Su, Emittance measurement and modeling for the Fermilab Booster. *Physical Review Special Topics-Accelerators and Beams*, *9*(1), 014202 (2006.).

[18] X.Yang, C.Ankenbrandt, J.MacLachlan, V.Lebedev, A Proposed Transition Scheme for the Longitudinal Emittance Control in the Fermilab Booster, FERMILAB-FN-0772 (2005)

[19] V.Lebedev, J.-F. Ostiguy, C.Bhat. Beam acceleration and transition crossing in the Fermilab Booster, in Proc. HB2016, Malmö, Sweden (2016), pp.160-163

[20] J.F.Ostiguy, C.Bhat, V.Lebedev. Modeling longitudinal dynamics in the Fermilab Booster Synchrotron, in Proc. IPAC2016, Busan, Korea (2016), pp.873-876.

[21] X.Yang, A.Drozhdin, W. Pellico, Momentum Spread Reduction at Beam Extraction from the Fermilab Booster at Slipstacking Injection to the Main Injector, in Proc. 2007 Particle Accelerator Conference, Albuquerque, New Mexico, USA (2007), pp.1733-1735.

[22] J. Wei, Synchrotrons and accumulators for high-intensity proton beams, Rev. Mod. Phys. **75** (2003) 1383.

[23] N.Mokhov, A. Drozhdin, P.Kasper, J.Lackey, E.Prebys, R.Webber. Fermilab booster beam collimation and shielding, in Proc. 2003 Particle Accelerator Conference, Portland, OR, USA (2003), vol. 3, pp. 1503-1505.

[24] V.Kapin, et al, Experimental Studies of Beam Collimation System in the Fermilab Booster, in Proc. NAPAC'16, Chicago, IL, USA (2016), pp.732-734.

[25] V.Shiltsev, F.Schmidt, Fermilab *beams-doc-6410* (June 4, 2018), unpublished.

[26] V.Shiltsev, Modern Physics Letters A, Mod. Phys. Lett.A 35 (10) 2030005 (2020); FERMILAB-PUB-20-087-AD-APC (2020)

[27] K.Seiya, et al, Beam Studies for the Proton Improvement Plan (PIP) - Reducing Beam Loss at the Fermilab Booster, in Proc. IPAC2015 (Richmond, VA, US), pp. 4027-4029

[28] J.Eldred, Physics Studies for High Intensity Proton Beams at the Fermilab Booster, in Proc. NAPAC2019 (Lansing, MI, USA, Sep.1-6, 2019), WEPLO10; Fermilab Beams-Doc-7610 (https://beamdocs.fnal.gov/).

[29] V.Shiltsev, Fermilab *beams-doc-7997* (Feb 11, 2020), unpublished.

[30] D.Johnson, et al., MEBT Laser Notcher (Chopper) for Booster Loss Reduction, Proc. HB2018 (Daejeon, Korea), pp.416-421 (2018).

[31] V. Shiltsev, et al., Beam-beam effects in the Tevatron, Phys. Rev. ST Accel. Beams 8, 101001 (2005)

[32] A.Burov, Convective instabilities of bunched beams with space charge, Phys. Rev. Accel. Beams 22, 034202 (2019).